PAPER

Check for updates

Degradation of herbicide atrazine in water by high voltage electrical discharge in comparison with Fenton oxidation and ultrasound treatments

Junting Hong, [iD] [ab] Nadia Boussetta,[a] Gérald Enderlin, [iD] [a] Franck Merlier[b] and Nabil Grimi*[a]

Atrazine, the most commonly used herbicide, has been reported to pollute the water environment and do harm to human health. It is thus urgent to find an efficient way to degrade atrazine. Although various advanced oxidation processes including high voltage electrical discharge (HVED) have been applied to degrade atrazine, the formation kinetics of its metabolites are still incomplete, and the detoxification of the degradation process remains to be clarified. Here, the degradation of atrazine by HVED was investigated, in comparison with traditional Fenton oxidation and ultrasound treatment. Nineteen metabolites of atrazine degradation were identified and quantified by high performance liquid chromatography coupled with high resolution mass spectrometry (HPLC-HRMS) techniques. Results show that HVED is more advantageous because of its high degradation rate for atrazine (89%), short processing time (1000 s, corresponding to 10 ms effective time), and the presence of the less toxic main metabolite hydroxyatrazine. Hydroxyl radicals ($^{\bullet}OH$) play an important role in atrazine degradation. Adding ferrous ions (Fe^{2+}) during HVED and ultrasound processes is beneficial for the degradation of atrazine, because of the $^{\bullet}OH$ radicals released from hydrogen peroxide (H_2O_2). Based on the formation kinetics of atrazine degradation metabolites, detailed mechanisms of atrazine degradation pathways were proposed.

Sustainability spotlight

The growing harvests have been increased by using pesticides extensively in response to the global food crisis. The health effects of excessive pesticide residues in drinking water may be severe. The widely used herbicide atrazine and its metabolites can remain in the environment for decades due to their stability and refractory degradation, becoming a major source of pollution. There is thus a strong need to efficiently degrade these persistent organic pollutants. Herein high voltage electrical discharges were applied to achieve rapid and deep degradation of recalcitrant pesticides. At the same time, we supplemented the data of pesticide degradation metabolites. Our work aligns with UN SDG 6 (water and sanitation) and SDG 12 (chemicals and waste management).

Introduction

As the production of agriculture has developed, pesticides have become increasingly important for controlling pests and weeds. However, the overuse of pesticides has been a source of concern for environmental pollution issues[1] and inherent impacts on human health.[2] Among these pesticides, atrazine is the most commonly used chlorotriazine herbicide to control weeds.[3] Atrazine's low biodegradability and high soil mobility make it persistent in non-agricultural soils,[4] as well as ground and surface water.[5] Atrazine was reported to be an endocrine disrupting chemical (EDC) posing a threat to the reproductive

system of mammals,[6] amphibians,[7] and fishes.[8] Although the European Union announced a ban on atrazine in 2003,[9] it is still extensively used in the United States,[10] Brazil,[11] and other countries.[12] The degradation of residual atrazine is thus becoming an urgent issue for environmental protection, especially for water security which is listed as a priority by the "European Green Deal" proposed by the European Commission. The degradation of chemically stable atrazine is challenging, and common water treatment technologies are limited by trace organic concentrations[13] and strict fouling control,[14] so there have been increasing efforts to develop efficient advanced oxidation processes,[3] such as Fenton/Fenton-like oxidation,[15–17] ultrasound[18–20] and so on. Among them, high voltage electrical discharge (HVED) has attracted more attention because of its advantages, high degradation efficiency and environmental friendliness.

During the HVED process, the electrical discharge plasma (a partially or fully ionized gas consisting of electrons, free radicals, ions and neutrals) is generated in a high voltage reactor.[21]

[a]Université de Technologie de Compiègne, ESCOM, TIMR (Integrated Transformations of Renewable Matter), Centre de Recherche Royallieu, CEDEX CS 60319, 60203 Compiègne, France. E-mail: nabil.grimi@utc.fr

[b]Université de Technologie de Compiègne, UPJV, CNRS, Enzyme and Cell Engineering, Centre de Recherche Royallieu, CEDEX CS 60319, 60203 Compiègne, France

This process is simultaneously affected by physical and chemical effects, generating various oxidizing species. The generated oxidizing species, such as hydroxy radicals ($^{\bullet}$OH), greatly promote the degradation of pollutants. Previous studies[22,23] demonstrated the viability of plasma for waste water treatment. To date, the application of HVED technology for atrazine degradation is still under development. Based on the plasma-phase distribution, the existing examples of atrazine degradation by HVED can be divided into two cases: one is direct discharge in water (electrohydraulic discharge),[24,25] and the other is discharge in the gas phase.[26–32] However, these reported works on the formation kinetics of atrazine degradation metabolites are incomplete.

Here, the energy was directly injected into the atrazine aqueous solution through a plasma channel formed by HVED between two submersed electrodes. It was aimed at investigating the ability of the HVED system to degrade atrazine in aqueous solution; comparing the results with a chemical degradation technique (Fenton oxidation) and physical degradation technique (ultrasound); studying the effect of Fe^{2+} on atrazine degradation; identifying atrazine degradation metabolites by high performance liquid chromatography coupled with high resolution mass spectrometry (HPLC-HRMS) analysis;[33] and proposing detailed mechanisms of atrazine degradation pathways based on the formation kinetics of atrazine degradation metabolites.

Experimental

Materials

LC-MS grade solvents and formic acid were bought from Biosolve Chimie (Dieuze, France). Atrazine and the internal standard Atrazine-D5 were bought from Sigma-Aldrich (St. Quentin Fallavier, France). In the preparation of the buffer solution, Milli-Q water purified with a Milli-Q system from Millipore (Millsheim, France) was used. Iron(II) sulfate heptahydrate ($FeSO_4 \cdot 7H_2O$) was purchased from Acros Organics with a purity of 99.5%. Hydrogen peroxide (H_2O_2) was purchased from Alfa Aesar with a purity of 35%.

Methods

Fig. 1 shows the experimental setup. The initial atrazine aqueous solutions of 20 mg L^{-1} were treated by three degradation methods including HVED, ultrasound and Fenton oxidation. After degradation, the treated fluid containing a mixture of atrazine and its metabolites was analyzed by HPLC-HRMS.
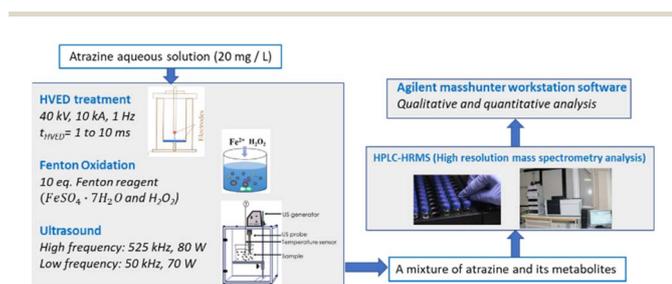
Qualitative and quantitative analyses were conducted using Agilent MassHunter Workstation software (version B.07.00, Agilent Technologies, Santa Clara, CA 95051, United States).

HVED treatment

Fig. 2 shows the schematic of the treatment chamber and pulse protocols for HVED. The high voltage electrical discharges were applied in a treatment chamber with a capacity of 1 L, using an electrical generator (Basis, Saint-Quentin, France) supplying a voltage of 40 kV, a current of 10 kA, and a frequency of 1 Hz. The generated pulses have a duration of approximately 10 μs. The average energy of an electric pulse supplied by the generator is $W_{1\ Pulse}$ = 200 J per pulse. The atrazine solution was introduced between two stainless steel electrodes. The first point electrode is connected to the generator; the second, a plane electrode, is connected to the ground. The electrical treatment consisted in applying n pulses (or n electrical discharges) in liquid. The total processing time was 1000 s (the total effective time was 10 ms).

A volume (250 or 500 mL) of the initial atrazine aqueous solution (20 mg L^{-1}, 0.093 mmol L^{-1}) was added in the treatment chamber, which was then treated by HVED. The initial concentration of ferrous sulfate $FeSO_4 \cdot 7H_2O$ was 0.93 mmol L^{-1} in HVED experiments adding Fe^{2+}. In addition, to study the effect of dissolved oxygen in the discharge system, the degradation of atrazine under an argon atmosphere was studied. A volume (500 mL) of the initial atrazine aqueous solution (20 mg L^{-1}, 0.093 mmol L^{-1}) was degassed and poured into the treatment chamber filled with an argon atmosphere, which was then treated by HVED. Samples were taken at 0, 100, 200, 400, 700 and 1000 s, and the corresponding effective time was 0, 1, 2, 4, 7, and 10 ms. With a frequency of 1 Hz, the corresponding number of pulses was 0, 100, 200, 400, 700 and 1000. The specific energy consumption of HVED, W_{HVED} (J L^{-1}), was calculated as follows:

$$W_{HVED} = (W_{1\ Pulse} \times n)/V \tag{1}$$

where $W_{1\ Pulse}$ is the average energy of one pulse (J per pulse); n is the number of pulses; and V is the treated volume (L).

Ultrasound treatment

For high frequency ultrasound, the atrazine solution (50 mL, 20 mg L^{-1}, 0.093 mmol L^{-1}) was poured into a 250 mL cup-shaped horn-type ultrasonic reactor purchased from SinapTec

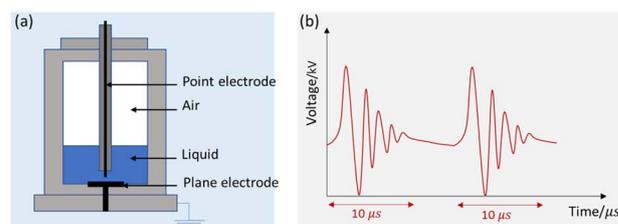**Fig. 1** Schema of the experimental procedures.

Fig. 2 Schematic representation of HVED: (a) treatment chamber and (b) pulsed protocols.

(Lezennes, France), and passed through a constant frequency of 525 kHz with 80 W power. The air flow was passed through the interlayer of the inner and outer walls to stabilize the temperature at 50 °C.

For low frequency ultrasound, an ultrasonic processor (Vibra-Cell 72434, Fisher Scientific, Illkirch, France) at 50 kHz frequency with 70 W power was applied. The atrazine solution (50 mL, 20 mg L^{-1}, 0.093 mmol L^{-1}) was poured into a 100 mL flat-bottom flask. The probe tip was placed at the center of the liquid. Temperature was kept at 50 °C using a water bath. The total treatment time was 8 h. Sampling was done at 0, 1, 2, 4 and 8 h. The initial concentration of ferrous sulfate $FeSO_4 \cdot 7H_2O$ was 0.93 mmol L^{-1} in ultrasound experiments adding Fe^{2+}. The specific energy consumption of ultrasound, W_{US} (J L^{-1}), was calculated as follows:

$$W_{US} = (P_{US} \times t)/V \tag{2}$$

where P_{US} is the power (W); t is the treatment time (s); and V is the treatment volume of the liquid (L).

Fenton oxidation treatment

Three initial atrazine solutions (50 mL, 20 mg L^{-1}, 0.093 mmol L^{-1}) were poured into three 100 mL flat-bottom flasks with magnets, and 10 eq., 5 eq. and 2 eq. of Fenton reagents (the ratio of the initial $FeSO_4 \cdot 7H_2O$ or H_2O_2 molar concentration to initial atrazine molar concentration was 10, 5 and 2, where $[FeSO_4 \cdot 7H_2O]_0 = [H_2O_2]_0 = 0.93$ mmol L^{-1}, 0.465 mmol L^{-1} and 0.186 mmol L^{-1}) were added, respectively. The reaction lasted for 8 h. Sampling was done at 0, 1, 2, 4 and 8 h.

Analysis by HPLC-HRMS

Atrazine and its metabolites were detected and quantified by HPLC-HRMS. A diode array detector (DAD) type HPLC system (Infinity 1290, Agilent Technologies, France) was connected with a micro-hybrid quadrupole time of flight (Q-TOF) and electrospray ionization (ESI) type mass spectrometer (Agilent 6538, Agilent Technologies, France). HLPC analyses were performed using a Thermo Hypersil Gold C18 (USP L1) column (100 × 2.1 mm, 1.9 μm, 175 A) at 40 °C. Eluents A and B consisted of 0.1% (v/v) formic acid in deionized water and 100% acetonitrile, respectively. The elution profile was 0–0.3 min 5% B, 0.3–1.7 min 5–30% B (linear gradient), 1.7–3.5 min 95% B (linear gradient), 3.5–4 min 95% B. The flow rate was 0.600 mL min^{-1}. The responses of compounds were measured in positive ESI mode with external calibration. By using the electrospray scan mode with a frequency of 5 Hz in the mass range of 50 to 1200 m/z and an electrospray voltage of 3800 V and fragment voltage of 110 V, positive ion electrospray mass spectra were obtained. The atomizing nitrogen temperature was 350 °C, the pressure was 30 psi, and the flow rate was 10 L min^{-1}.
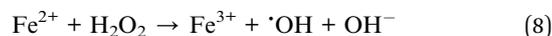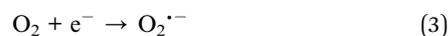
Results and discussion

Atrazine and its detected metabolites

The abbreviations of atrazine and its detected metabolites are shown in Table 1.

Atrazine degradation by HVED

In Fig. 3, atrazine degradation rates by HVED as a function of the effective time are given for different experimental conditions. As the results show, for the atrazine solution of 500 mL, within 2 ms of discharge, the degradation rate of atrazine in an argon atmosphere was lower than that in an air atmosphere, indicating that dissolved oxygen might enhance the degradation of atrazine in the discharge process. According to ref. 34 and 35, dissolved oxygen can react with the high-energy electrons and produce superoxide radical anions $O_2^{\cdot-}$ (eqn (3)) that can degrade atrazine. So, it would be better to conduct the discharge experiments directly under the air.

In addition, four comparative HVED experiments were conducted in different treatment volumes with or without Fe^{2+} addition. In the same treatment volume, adding Fe^{2+} enhanced the degradation rate of atrazine. This result is consistent with results from the literature;[24] ferrous sulfate $FeSO_4 \cdot 7H_2O$ added to the pulsed electrical discharge reactor improved the degradation of atrazine due to the classical Fenton reaction. During the electrical discharge process, the electron impact of H_2O molecules is the main way to produce hydroxy radicals $^{\cdot}OH$ (eqn (4)).[36] Reactions between radicals can produce hydrogen, hydrogen peroxide, or re-formed water (eqn (5)–(7)). These self-quenching reactions lead to the consumption of $^{\cdot}OH$ radicals, which inhibit atrazine degradation. However, adding ferrous ions (Fe^{2+}) reduced these $^{\cdot}OH$ radicals' consumption via the Fenton reaction (eqn (8)). The results also show that a higher degradation rate of atrazine was observed for lower treatment volume. The specific energy consumption per unit pulse (J L^{-1} per pulse) is 400 J L^{-1} per pulse for 500 mL, and 800 J L^{-1} per pulse for 250 mL. At the same treatment time, the pulse number is the same; the specific energy consumption is higher for the lowest treated volume, thus enhancing the degradation rate of atrazine.

$$O_2 + e^- \rightarrow O_2^{\cdot-} \tag{3}$$

$$H_2O + e^- \rightarrow {}^{\cdot}OH + {}^{\cdot}H + e^- \tag{4}$$

$${}^{\cdot}H + {}^{\cdot}H \rightarrow H_2 \tag{5}$$

$${}^{\cdot}OH + {}^{\cdot}OH \rightarrow H_2O_2 \tag{6}$$

$${}^{\cdot}H + {}^{\cdot}OH \rightarrow H_2O \tag{7}$$

$$Fe^{2+} + H_2O_2 \rightarrow Fe^{3+} + {}^{\cdot}OH + OH^- \tag{8}$$

Atrazine degradation by ultrasound

Fig. 4 shows the effect of frequency and Fe^{2+} on atrazine degradation by ultrasound. The degradation rates of atrazine by HFUS (525 kHz) were much higher than those with LFUS (50 kHz). The frequency and power of irradiation determine the physical characteristics of ultrasonication, such as bubble sizes and collapse temperatures. A higher frequency causes higher turbulence because the bubbles are more likely to implode, enhancing mass transfers. The results also showed that adding Fe^{2+} greatly improved atrazine degradation regardless of the frequency.
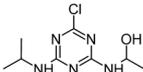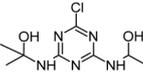
Table 1 Atrazine and its detected metabolites

Abbreviation	Structure	Formula	Name	m/z	Retention time (min)	Detected process
ATZ		$C_8H_{14}ClN_5$	Atrazine	216.1010	2.558	All treatments (HFUS, LFUS, Fenton, HVED)
DEA		$C_6H_{10}ClN_5$	Deethylatrazine	188.0698	1.910	
DIA		$C_5H_8ClN_5$	Deisopropylatrazine	174.0541	1.620	
CVIT		$C_8H_{12}ClN_5$	6-Chloro-N2-ethenyl-N4-(propan-2-yl)-1,3,5-triazine-2,4-diamine	214.0854	2.070	
CDIT		$C_8H_{12}ClN_5O$	N-[4-Chloro-6-(isopropylamino)-1,3,5-triazin-2-yl]acetamide	230.0804	2.091	
ODIT		$C_8H_{13}N_5O_2$	N-[4-Hydroxy-6-(isopropylamino)-1,3,5-triazin-2-yl]acetamide	212.1142	1.213	
CDET		$C_7H_{10}ClN_5O$	N-[4-Chloro-6-(ethylamino)-1,3,5-triazin-2-yl]acetamide	216.0647	1.820	
ODET		$C_7H_{11}N_5O_2$	N-[6-(Ethylamino)-4-oxo-1,4-dihydro-1,3,5-triazin-2-yl]acetamide	198.0986	1.082	
HA		$C_8H_{15}N_5O$	Hydroxyatrazine	198.1350	1.233	
DEHA		$C_6H_{11}N_5O$	Deethylhydroxyatrazine	170.1037	0.810	All treatments except Fenton
DIHA		$C_5H_9N_5O$	Deisopropylhydroxyatrazine	156.0880	0.560	
CDAT		$C_5H_6ClN_5O$	N-(4-Amino-6-chloro-1,3,5-triazin-2-yl)acetamide	188.0334	1.264	
OEAT		$C_5H_7N_5O_2$	N-(4-Amino-6-hydroxy-1,3,5-triazin-2-yl)acetamide	170.0673	0.727	All treatments except HVED
CDDT		$C_7H_8ClN_5O_2$	N,N'-(6-Chloro-1,3,5-triazine-2,4-diyl)diacetamide	230.0440	1.451	
ODDT		$C_7H_9N_5O_3$	N,N'-(6-Hydroxy-1,3,5-triazine-2,4-diyl)diacetamide	212.0778	1.141	
DDA		$C_3H_4ClN_5$	Didealkylatrazine	146.0228	1.023	All treatments except LFUS
AM		$C_3H_5N_5O$	Ammeline	128.0567	0.490	
CBOI		$C_3H_5N_3O_4$	1-Carboxybiuret	148.0353	0.416	HVED (very trace amounts)

Table 1 (*Contd.*)

Abbreviation	Structure	Formula	Name	m/z	Retention time (min)	Detected process
CNIT		$C_8H_{14}ClN_5O$	1-({4-Chloro-6-[(propan-2-yl)amino]-1,3,5-triazin-2-yl}amino)ethan-1-ol	232.0960	1.868	
HAHT		$C_8H_{14}ClN_5O_2$	2-({4-Chloro-6-[(1-hydroxyethyl)amino]-1,3,5-triazin-2-yl}amino)propan-2-ol	248.0909	2.212	Fenton
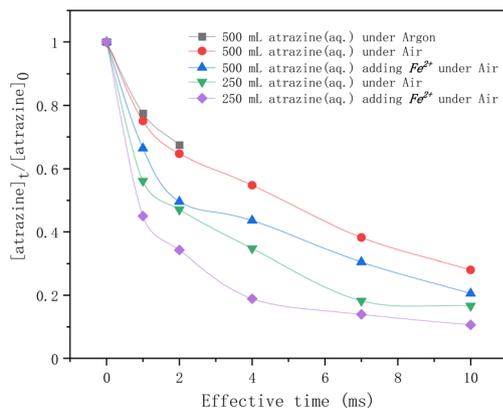
Fig. 3 Time profiles of atrazine degradation by HVED in different treatment volumes adding Fe^{2+} or not.
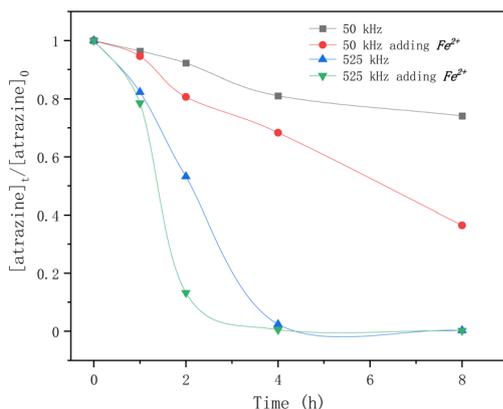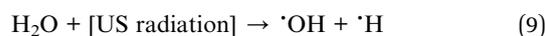

Fig. 4 Time profiles of atrazine degradation by ultrasound at different frequencies adding Fe^{2+} or not.

In atrazine aqueous solution, the main sono-chemical dissociation processes are homolytic cleavage of water to release $^{\cdot}OH$ and $^{\cdot}H$ radicals (eqn (9)).

$$H_2O + [\text{US radiation}] \rightarrow {}^{\cdot}OH + {}^{\cdot}H \qquad (9)$$

But the self-combination of the produced $^{\cdot}OH$ radicals (eqn (6)), with a second-order rate constant of 5×10^9 M^{-1} s^{-1},[37] is faster than the degradation of atrazine with a rate constant of 2.4×10^9 M^{-1} s^{-1}.[24] The addition of Fe^{2+} is beneficial for the degradation of atrazine by releasing the $^{\cdot}OH$ radical from its self-combination product hydrogen peroxide by the classical Fenton reaction (eqn (8)).

Atrazine degradation by Fenton oxidation

In Fig. 5, the equivalents of the Fenton reagents were studied in the degradation of atrazine by Fenton oxidation. Within the first 5 hours, atrazine was degraded more rapidly by adding 5 eq. and 10 eq. of Fenton reagents. After 5 h, atrazine was nearly completely degraded regardless of the number of equivalents of Fe^{2+}. For 5 eq. and 10 eq. of Fenton reagents, the elimination of atrazine was rapid within the first hour, and tended to slow down until reaching equilibrium. For 2 eq. of Fenton reagents, the degradation rate of atrazine was rapid in the first hour, but flattened in the second hour, and later it became rapid again until it reached equilibrium. The reason may be due to the consumption of Fe^{2+} and the generation of $^{\cdot}OH$ radicals.

As mentioned above, in the classical Fenton reaction, ferrous ions (Fe^{2+}) react with hydrogen peroxide to form $^{\cdot}OH$ radicals which are the reactive oxygen species for atrazine degradation. When most of the ferrous ions (Fe^{2+}) are converted to ferric ions (Fe^{3+}), the generated ferric ions (Fe^{3+}) tend to react with hydrogen peroxides to release ferrous ions (Fe^{2+}) (eqn (10)). According to ref. 38, the reaction rate constants of eqn (8) and (10) are 76 M^{-1} s^{-1} and 0.01 M^{-1} s^{-1} respectively. The reaction between $^{\cdot}OH$ radicals and atrazine is instantaneous (eqn (11)), and its reaction rate constant is 2.4×10^9 M^{-1} s^{-1}.[24] Therefore,
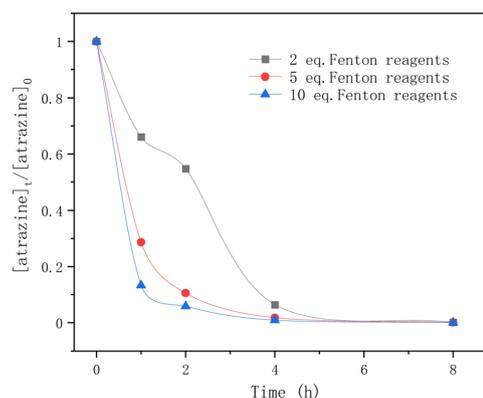

Fig. 5 Time profiles of atrazine degradation for different Fenton reagent equivalents.

for 2 eq. of Fe^{2+}, at the beginning, the $^{\bullet}OH$ radicals formed by the Fenton reaction quickly degraded atrazine.

As Fe^{2+} was consumed, the formation of the $^{\bullet}OH$ radicals was inhibited and the degradation rate of atrazine was flattened. Then the release of Fe^{2+} from Fe^{3+} restarted the Fenton reaction and again provided $^{\bullet}OH$ radicals for atrazine degradation. For 5 eq. and 10 eq. of Fe^{2+}, sufficient Fe^{2+} ensured the continuous generation of $^{\bullet}OH$ radicals from hydrogen peroxides, so the degradation rate of atrazine was very fast until it reached equilibrium. In this study, having a large number of equivalents of Fe^{2+} was found to favor atrazine degradation.

$$Fe^{3+} + H_2O_2 \rightarrow Fe^{2+} + HO_2^{\bullet} + H^+ \qquad (10)$$

$$^{\bullet}OH + atrazine \rightarrow products \qquad (11)$$
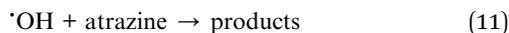
Formation kinetics of metabolites

Fig. 6 shows the formation kinetics of metabolites during atrazine degradation by different treatments. The chemical structures of these metabolites represented by abbreviations are shown in Table 1. In 525 kHz ultrasound treatment (Fig. 6(a) and (b)), dealkylation and carbonylation products such as DIA, CDIT and CDAT are the major metabolites while the dechlorination products are less present, and adding Fe^{2+} improved the production of dealkylation products DEA and DIA. In low frequency ultrasound treatment (Fig. 6(c)), dealkylation and carbonylation products CDIT and CDET as well as the dechlorination product ODIT are the main metabolites. In Fenton oxidation (Fig. 6(d)), the

formation kinetics of metabolites were more variable over time, and it produced the final main product ammeline (AM).

In HVED treatment (Fig. 6(e) and (f)), the dechlorination product hydroxyatrazine (HA) was the main product no matter whether Fe^{2+} was added or not. Notably, the ring cleavage product carboxybiuret (CBOI) was detected in the HVED treatment, which is not shown below (Fig. 6(e) and (f)) due to its trace amounts. This implies that HVED treatment is a potential degradation pathway for s-triazine ring-cleavage. In the future, we will make more effort to promote this s-triazine ring-cleavage so as to pursue mineralization.

Proposed mechanism

Based on the formation kinetics of metabolites, the mechanism of atrazine degradation is proposed in Fig. 7. $^{\bullet}OH$ radicals may attack atrazine molecules in different positions, including attacking the alkylamino side chains,[39] or attacking the *ipso*-position of the chlorine substituent.[40] So, we propose four pathways I, II, III and IV for atrazine degradation according to different positions of $^{\bullet}OH$ attack.

Pathway I. An attack of the $^{\bullet}OH$ radical at the *ipso*-position of the chlorine substituent might lead to a geminal chlorohydrine, yielding an HO-adduct by elimination of an HCl molecule.[39,41] The dechlorination-hydroxylated product HA was detected in HVED and HFUS processes, and it could be further degraded into DEHA and DIHA, followed by the generation of deeper oxidation products. It is noteworthy that hydroxylated atrazine degradation products were found to be less toxic.[42] So, the
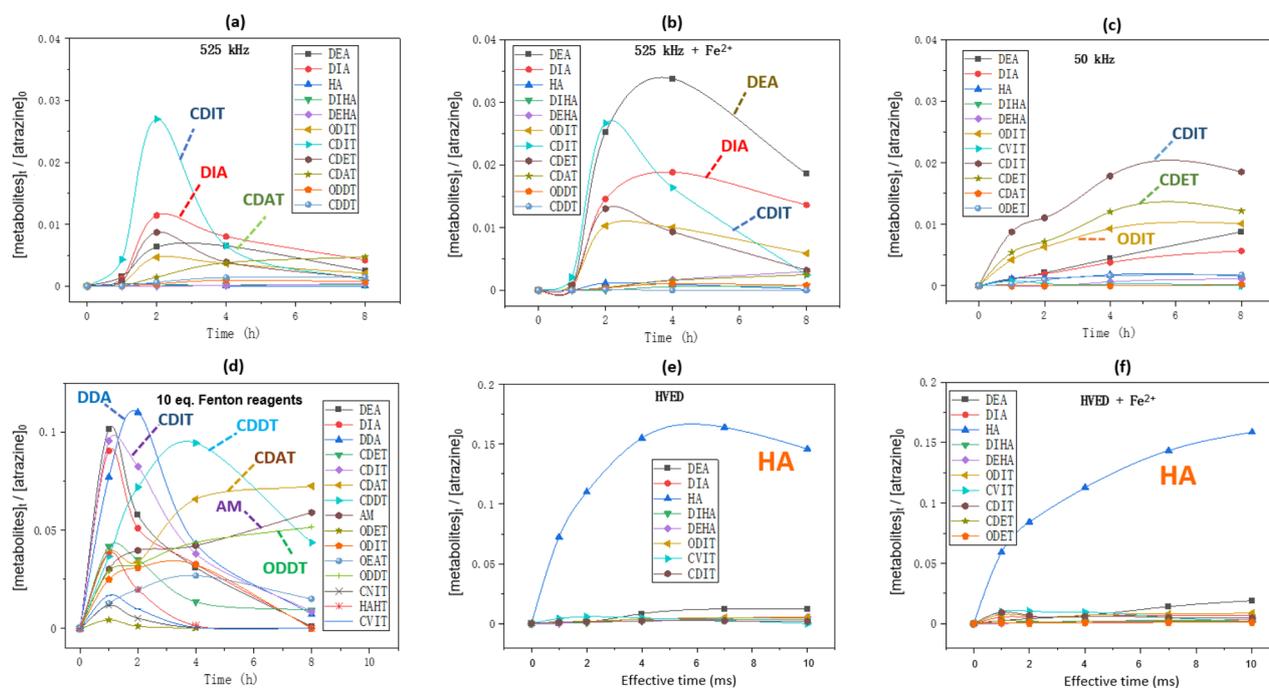

Fig. 6 Formation kinetics of metabolites during atrazine degradation: (a and b) 50 mL of atrazine solution was treated by ultrasound at 525 kHz with or without addition of 10 eq. of $FeSO_4 \cdot 7H_2O$; (c) 50 mL of atrazine solution was treated by ultrasound at 50 kHz with or without addition of 10 eq. of $FeSO_4 \cdot 7H_2O$; (d) 50 mL of atrazine solution was added by 10 eq. of H_2O_2 and 10 eq. of $FeSO_4 \cdot 7H_2O$; (e and f) 250 mL of atrazine solution was treated by HVED with or without addition of 10 eq. of $FeSO_4 \cdot 7H_2O$. Initial atrazine concentration is always 0.093 mmol L^{-1}.
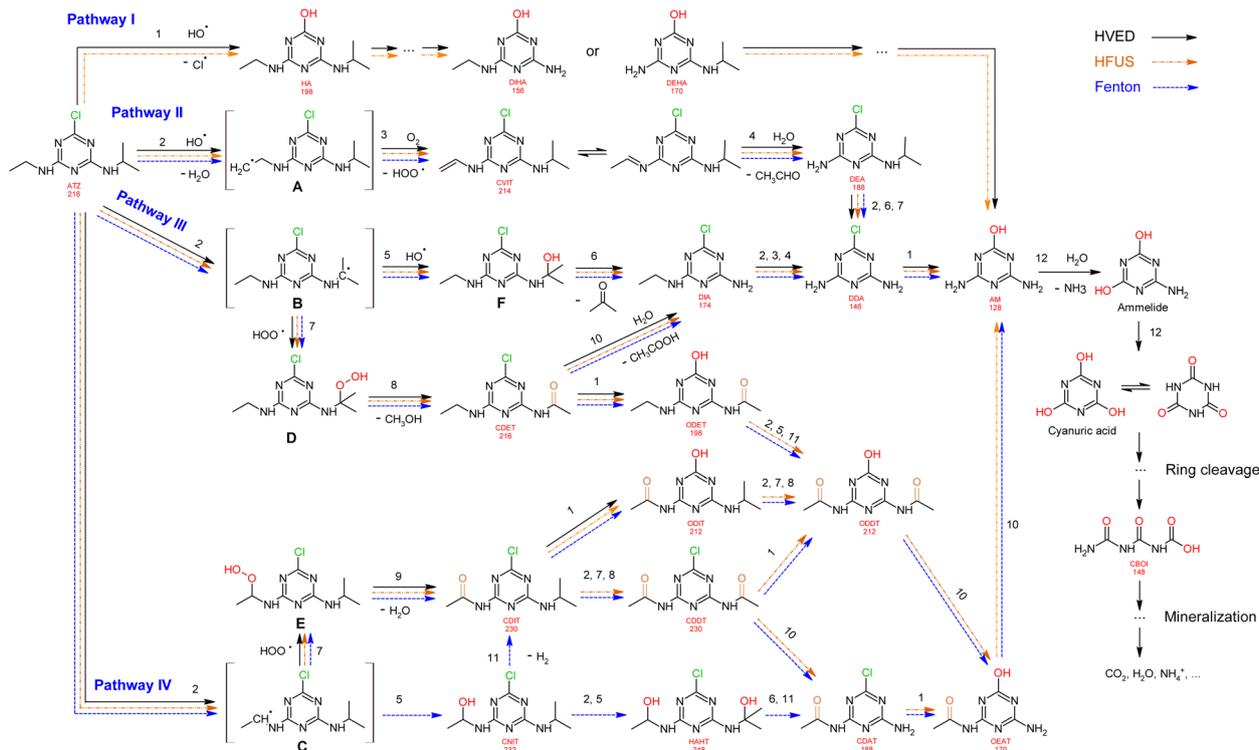
Fig. 7 Proposed degradation pathways of atrazine.

HVED process appears to be more desirable for atrazine detoxification, since it mainly produced the hydroxylated product HA (Fig. 6(e) and (f)).

Pathway II. Radical ˙OH attacks the β-C adjacent to the N atom on the ethylamino side chain, generating carbon-center radical **A** through H-atom abstraction. The carbon-centered radical **A** could be attacked by dissolved O_2 to form a perhydroxyl radical (HOO˙) and olefination product CVIT. Further oxidation of CVIT might lead to the formation of acetaldehyde and dealkylated product DEA.[43] CVIT and DEA were both detected in HVED, HFUS and Fenton processes.

Pathway III. Radical ˙OH attacks the α-C adjacent to the N atom on the isopropylamino side chain, generating carbon-center radical **B** through H-atom abstraction. The carbon-center radical **B** could be further attacked by ˙OH to form alkylic-hydroxylation intermediate **F**, leading to the generation of acetone and dealkylated product DIA. Another way, the perhydroxyl radical (HOO˙) might attack the carbon-center radical **B**, inducing the generation of atrazine-peroxide intermediate **D** which might produce methanol and alkylic-oxidation product CDET.[40] CDET might produce dechlorination-hydroxylated product ODET or dealkylated product DIA through the hydrolysis of the amide group.[41] Both DIA and DEA mentioned in pathway II could be further oxidized to the fully dealkylated DDA and its dechlorination-hydroxylated product ammeline (AM). CDET, ODET, DIA, DDA and AM were detected in HVED, HFUS and Fenton processes. But DDA and AM were not found in the LFUS process, indicating that low frequency ultrasound is not conducive to deeper oxidation.

Pathway IV. Radical ˙OH attacks the α-C adjacent to the N atom on the ethylamino side chain, generating carbon-center radical **C** through H-atom abstraction. The carbon-center radical **C** could be attacked by ˙OH to form alkylic-hydroxylation intermediate CNIT. Then, intermediate CNIT might produce alkylic-oxidation product CDIT through H-abstraction,[44] or produce another alkylic-hydroxylation intermediate HAHT.[18] CNIT and HAHT were detected in the Fenton process. HAHT might be further oxidized to the dealkylated product CDAT and its dechlorination-hydroxylated product OEAT. Another way, the carbon-center radical **C** could be attacked by HOO˙ and form atrazine-peroxide intermediate **E**, followed by the generation of CDIT. CDIT could produce its dechlorination-hydroxylated product ODIT, or be further oxidized to CDDT, followed by the generation of ODDT and CDAT. Previous studies[45,46] have shown that carboxybiuret (CBOI) formed from ring cleavage of cyanuric acid might undergo spontaneous decarboxylation to biuret, which could be further mineralized into small molecules such as CO_2, H_2O, NH_3, etc. However, the specific mechanism of ring cleavage is still uncertain, which will be the content of future research. In the HVED process, CDDT, ODDT, CDAT and OEAT were not detected, but AM and the ring cleavage product CBOI were detected, indicating that HVED treatment is more favorable for mineralization.

In the final degradation stage of these four pathways, the dechlorination-hydroxylated product AM is generated, and its deeper oxidations may lead to the formation of the ring cleavage product CBOI, which could be further mineralized into small

Table 2 Comparison of high frequency ultrasound, Fenton oxidation and HVED treatments

Technologies	Degradation rate of atrazine	Main formed metabolites	Specific energy consumption $(kJ\ L^{-1})$
Ultrasound (525 kHz)	47% (treatment time 2 h)	DIA	11 520 kJ L^{-1}
Ultrasound (525 kHz) + Fe^{2+}	87% (treatment time 2 h)	DEA	
Fenton oxidation (10 eq. of Fenton reagents)	>95% (treatment time 2 h)	AM	
HVED (250 mL ATZ solution)	83% (effective time 10 ms)	HA	800 kJ L^{-1}
HVED + Fe^{2+} (250 mL atrazine solution)	89% (effective time 10 ms)		

molecules such as CO_2, H_2O, NH_3, *etc.* However, the specific mechanism of ring cleavage is still unclear and needs further study.

Comparison of different degradation techniques

In Table 2, high frequency ultrasound, Fenton oxidation and HVED treatments are compared in terms of degradation rate of atrazine, main formed metabolites and specific energy consumption. The toxicity ranking of atrazine and its metabolites is ATZ > DEA > DIA > AM > DDA > HA.[3] For high frequency ultrasound treatment, after 2 h, the atrazine degradation rate was unfavorable at only 47%, and adding ferrous ions doubled the degradation rate to 87%, but the disadvantages still exist with the presence of toxic main metabolites and a high energy consumption. For Fenton oxidation, although it reached the highest atrazine degradation rate of 95%, it produced toxic main metabolite AM. For HVED, adding ferrous ions enhanced the degradation rate of atrazine from 83% to 89%, due to the Fenton reaction, in which ferrous ions reacted with the hydrogen peroxide produced by the discharge.[24] By comparison, HVED is more advantageous because of the high degradation efficiency in short treatment time, the presence of less toxic main metabolite HA and the lower energy consumption.

Conclusions

An innovative atrazine degradation method was reported using high voltage electrical discharge (HVED). The HVED method was compared with the traditional atrazine degradation method, Fenton oxidation and ultrasound treatment at high or low frequency. HVED treatment was more advantageous, since atrazine can be mostly degraded (89%) with the addition of ferrous ions, in short effective time (10 ms), while the treatment time of the Fenton oxidation and ultrasound process lasted for 2 h. Besides, the main generated metabolite hydroxyatrazine (HA) in the HVED process was less toxic than the deethylatrazine (DEA) and deisopropylatrazine (DIA) generated in the ultrasound process, and ammeline (AM) generated in the Fenton process. Also, when the degradation rates of atrazine were around 87%, the specific energy requirement of HVED (800 kJ L^{-1}) was much lower than that of ultrasound at high frequency (11 520 kJ L^{-1}). In addition, ferrous ions (Fe^{2+}) promoted the degradation of atrazine in those three treatments *via* the Fenton reaction with hydrogen peroxide (H_2O_2), releasing the important reactive oxygen species, hydroxyl radicals ˙OH. Finally, the formation kinetics of metabolites and the proposed pathways

may provide a reference for future research on atrazine degradation.

Author contributions

Junting Hong: conceptualization, methodology, data analysis, writing – original draft preparation. Nadia Boussetta: methodology, writing – reviewing & editing. Gérald Enderlin: writing – reviewing & editing. Franck Merlier: conceptualization, data analysis, writing – reviewing & editing and supervision. Nabil Grimi: conceptualization, writing – reviewing & editing and supervision.

Conflicts of interest

There are no conflicts to declare.

Acknowledgements

References

1 D. Munaron, B. Mérigot, V. Derolez, N. Tapie, H. Budzinski and A. Fiandrino, *Sci. Total Environ.*, 2022, **867**, 161303.

2 B. G. Silva Pinto, T. K. Marques Soares, M. Azevedo Linhares and N. Castilhos Ghisi, *Sci. Total Environ.*, 2020, **748**, 141382.

3 J. Hong, N. Boussetta, G. Enderlin, F. Merlier and N. Grimi, *Foods*, 2022, **11**, 2416.

4 F. Giannini-Kurina, J. Borello, I. Cañas, S. Hang and M. Balzarini, *Soil Tillage Res.*, 2022, **219**, 105320.

5 T. Bohn, E. Cocco, L. Gourdol, C. Guignard and L. Hoffmann, *Food Addit. Contam.: Part A*, 2011, **28**, 1041–1054.

6 Y. Yun, S. Lee, C. So, R. Manhas, C. Kim, T. Wibowo, M. Hori and N. Hunter, *Environ. Health Perspect.*, 2022, **130**, 117007.

7 T. B. Hayes, V. Khoury, A. Narayan, M. Nazir, A. Park, T. Brown, L. Adame, E. Chan, D. Buchholz, T. Stueve and S. Gallipeau, *Proc. Natl. Acad. Sci. U. S. A.*, 2010, **107**, 4612–4617.

8 S. E. Wirbisky and J. L. Freeman, *Toxics*, 2015, **3**, 414–450.

9 J. Bethsass and A. Colangelo, *Int. J. Occup. Environ. Health*, 2006, **12**, 260–267.

10 J. A. Rusiecki, A. De Roos, W. J. Lee, M. Dosemeci, J. H. Lubin, J. A. Hoppin, A. Blair and M. C. R. Alavanja, *JNCI, J. Natl. Cancer Inst.*, 2004, **96**, 1375–1382.

11 E. M. Brovini, B. C. T. de Deus, J. A. Vilas-Boas, G. R. Quadra, L. Carvalho, R. F. Mendonça, R. d. O. Pereira and S. J. Cardoso, *Sci. Total Environ.*, 2021, **771**, 144754.

12 J. T. Sun, L. L. Pan, Y. Zhan, D. C. W. Tsang, L. Z. Zhu and X. D. Li, *Environ. Geochem. Health*, 2017, **39**, 369–378.

13 X. Cheng, H. Liang, A. Ding, X. Tang, B. Liu, X. Zhu, Z. Gan, D. Wu and G. Li, *Water Res.*, 2017, **113**, 32–41.

14 P. Wang, Y. Yin, Y. Guo and C. Wang, *RSC Adv.*, 2016, **6**, 10615–10624.

15 Y. Liu and J. Wang, *Chem. Eng. J.*, 2023, **466**, 143147.

16 S. Wang and J. Wang, *ACS ES&T Water*, 2022, **2**, 852–862.

17 S. Wang, G. Yu and J. Wang, *Chemosphere*, 2023, **317**, 137889.

18 L. J. Xu, W. Chu and N. Graham, *J. Hazard. Mater.*, 2014, **275**, 166–174.

19 X. Lu, W. Qiu, J. Peng, H. Xu, D. Wang, Y. Cao, W. Zhang and J. Ma, *J. Hazard. Mater.*, 2021, **403**, 123915.

20 S. M. R. Azam, H. Ma, B. Xu, S. Devi, M. A. B. Siddique, S. L. Stanley, B. Bhandari and J. Zhu, *Trends Food Sci. Technol.*, 2020, **97**, 417–432.

21 B. Jiang, J. Zheng, S. Qiu, M. Wu, Q. Zhang, Z. Yan and Q. Xue, *Chem. Eng. J.*, 2014, **236**, 348–368.

22 M. R. Ghezzar, F. Abdelmalek, M. Belhadj, N. Benderdouche and A. Addou, *J. Hazard. Mater.*, 2009, **164**, 1266–1274.

23 V. I. Grinevich, E. Y. Kvitkova, N. A. Plastinina and V. V. Rybkin, *Plasma Chem. Plasma Process.*, 2011, **31**, 573–583.

24 S. Mededovic and B. R. Locke, *Ind. Eng. Chem. Res.*, 2007, **46**, 2702–2709.

25 Y. Shang, N. Jiang, Z. Liu, C. Li, H. Sun, H. Guo, B. Peng and J. Li, *Chem. Eng. J.*, 2023, **452**, 139342.

26 J. Feng, L. Jiang, D. Zhu, K. Su, D. Zhao, J. Zhang and Z. Zheng, *Environ. Sci. Pollut. Res.*, 2016, **23**, 9204–9214.

27 M. Hijosa-Valsero, R. Molina, H. Schikora, M. Müller and J. M. Bayona, *J. Hazard. Mater.*, 2013, **262**, 664–673.

28 T. Shen, X. Wang, P. Xu, C. Yang, J. Li, P. Wang and G. Zhang, *Environ. Res.*, 2022, **212**, 113287.

29 P. Vanraes, G. Willems, A. Nikiforov, P. Surmont, F. Lynen, J. Vandamme, J. Van Durme, Y. P. Verheust, S. W. H. Van Hulle, A. Dumoulin and C. Leys, *J. Hazard. Mater.*, 2015, **299**, 647–655.

30 Q. Wang, A. Zhang, P. Li, P. Héroux, H. Zhang, X. Yu and Y. Liu, *J. Hazard. Mater.*, 2021, **403**, 124087.

31 N. Wardenier, Z. Liu, A. Nikiforov, S. W. H. Van Hulle and C. Leys, *Chemosphere*, 2019, **234**, 715–724.

32 D. Zhu, L. Jiang, R.-l. Liu, P. Chen, L. Lang, J.-w. Feng, S.-j. Yuan and D.-y. Zhao, *Chemosphere*, 2014, **117**, 506–514.

33 J. Hong, N. Boussetta, G. Enderlin, N. Grimi and F. Merlier, *Molecules*, 2022, **27**, 9021.

34 G. Nie, L. Xiao, J. Bi, S. Wang and X. Duan, *Appl. Catal., B*, 2022, **315**, 121584.

35 X. Wang, Y. Wang, N. Chen, Y. Shi and L. Zhang, *Chemosphere*, 2020, **244**, 125568.

36 P. Lukes and B. R. Locke, *J. Phys. D: Appl. Phys.*, 2005, **38**, 4074.

37 Y. Hu, Z. Zhang and C. Yang, *Ultrason. Sonochem.*, 2008, **15**, 665–672.

38 D. R. Grymonpré, A. K. Sharma, W. C. Finney and B. R. Locke, *Chem. Eng. J.*, 2001, **82**, 189–207.

39 A. Tauber and C. von Sonntag, *Acta Hydrochim. Hydrobiol.*, 2000, **28**, 15–23.

40 C. A. Aggelopoulos, D. Tataraki and G. Rassias, *Chem. Eng. J.*, 2018, **347**, 682–694.

41 Y. Ji, C. Dong, D. Kong, J. Lu and Q. Zhou, *Chem. Eng. J.*, 2015, **263**, 45–54.

42 R. N. Lerch, W. W. Donald, Y.-X. Li and E. E. Alberts, *Environ. Sci. Technol.*, 1995, **29**, 2759–2768.

43 J. A. Khan, X. He, N. S. Shah, H. M. Khan, E. Hapeshi, D. Fatta-Kassinos and D. D. Dionysiou, *Chem. Eng. J.*, 2014, **252**, 393–403.

44 X. Kong, L. Wang, Z. Wu, F. Zeng, H. Sun, K. Guo, Z. Hua and J. Fang, *Water Res.*, 2020, **177**, 115784.

45 A. K. Bera, K. G. Aukema, M. Elias and L. P. Wackett, *Sci. Rep.*, 2017, **7**, 45277.

46 J. L. Murphy, M. J. Arrowood, X. Lu, M. C. Hlavsa, M. J. Beach and V. R. Hill, *Environ. Sci. Technol.*, 2015, **49**, 7348–7355.